Vortex lattices in binary Bose-Einstein condensates with dipole-dipole interactions

Ramavarmaraja Kishor Kumar,[1] Lauro Tomio,[2,3] Boris A. Malomed,[4,5] and Arnaldo Gammal[1]

[1]*Instituto de Física, Universidade de São Paulo, 05508-090 São Paulo, São Paulo, Brazil*
[2]*Instituto de Física Teórica, Universidade Estadual Paulista, 01156-970 São Paulo, São Paulo, Brazil*
[3]*InstitutoTecnológico de Aeronáutica, DCTA,12.228-900 São José dos Campos, São Paulo, Brazil*
[4]*Department of Physical Electronics, School of Electrical Engineering, Faculty of Engineering, Tel Aviv University, Tel Aviv 69978, Israel*
[5]*ITMO University, Saint Petersburg 197101, Russia*

We study the structure and stability of vortex lattices in two-component rotating Bose-Einstein condensates with intrinsic dipole-dipole interactions and contact interactions. To address experimentally accessible coupled systems, we consider ^{164}Dy-^{162}Dy and ^{168}Er-^{164}Dy mixtures, which feature different miscibilities. The corresponding dipole moments are $\mu_{\text{Dy}} = 10\mu_{\text{B}}$ and $\mu_{\text{Er}} = 7\mu_{\text{B}}$, where μ_{B} is the Bohr magneton. For comparison we also discuss a case where one of the species is nondipolar. Under a large aspect ratio of the trap, we consider mixtures in the pancake-shaped format, which are modeled by effective two-dimensional coupled Gross-Pitaevskii equations, with a fixed polarization of the magnetic dipoles. Then, the miscibility and vortex-lattice structures are studied by varying the coefficients of the contact interactions (assuming the use of the Feshbach-resonance mechanism) and the rotation frequency. We present phase diagrams for several types of lattices in the parameter plane of the rotation frequency and the ratio of inter- and intraspecies scattering lengths. The vortex structures are found to be diverse for the more miscible ^{164}Dy-^{162}Dy composition, with a variety of shapes, whereas for the less miscible case of ^{168}Er-^{164}Dy, the lattice patterns mainly feature circular or square formats.

I. INTRODUCTION

In Bose-Einstein condensates (BECs), quantized vortices emerge above a certain critical rotation frequency [1], which may be imposed by techniques such as rotating traps, laser stirring, and the addition of an oscillatory excitation to the trapping potential [2]. Experiments for vortices have also been performed with multicomponent BECs. In this regard, we can mention Ref. [3], as well as works cited in the recent review by Martin *et al.* [4]. In particular, the study of vortices in binary condensates is interesting due to the fact that interspecies interactions produce diverse vortex structures in addition to the fundamental Abrikosov's triangular lattice, such as square-shaped and coreless lattices, domain walls, droplets, and isolated density peaks in the two-component mixtures [5–8].

Recent experiments with ^{168}Er and ^{164}Dy condensates have also stimulated interest in properties of quantum droplets that can be created in dipolar BECs [9–11]. These studies have revealed that the droplets are self-trapped as many-body states in bosonic gases, supported by the balance between attractive and repulsive forces in these settings. With the attractive forces being provided by dipole-dipole interactions (DDIs), the repulsive cases are induced by the beyond-mean-field quantum fluctuation effects, known as Lee-Huang-Yang corrections. They are also used to predict stable droplets in nondipolar two-component systems [12–14], which have been created very recently in experiments [15–17].

The objective of this paper is to study rotational regimes of two-component dipolar BECs. Previous studies dealing with vortices in dipolar BECs have explained the role of DDIs in the formation of vortices, as reported in the review [4]. In particular, the theoretical analysis dealt with the calculation of the critical rotation frequency and vortex structures under the action of the DDI [18–20]. In the two-component setting with one dipolar component and the other one carrying no dipole moments, the dipolar component features a smaller critical rotation frequency than its nondipolar counterpart, and the dipolar component produces a larger number of vortices than the nondipolar one, at the same rotation frequency [21].

In general, vortex states in binary BECs are strongly affected by the (im)miscibility. Completely miscible settings feature triangular, square-shaped, and rectangular vortex lattices, depending on the rotation frequency. On the other hand, immiscible binary condensates support bound states of vortices, stripes, and vortex sheets (domain walls) [5,6]. In this regard, to explore vortex structures in binary condensates, we rely on results obtained in a previous study, reported in Ref. [22], for the miscibility of two-component dipolar systems. In this reference, by considering stability requirements and miscibility properties, it was found more appropriate to consider pancake-shaped symmetry for the trap, varying the inter- and intraspecies contact interactions to modify the miscibility properties.

In the present work, we report manifestations of the miscibility-immiscibility transition in dipolar mixtures in terms of vortex-lattice configurations. We address vortex-lattice states in two-component BECs under the action of the DDIs, by considering the same dipolar systems previously studied in Ref. [22]. Following that, our analysis is performed for a pancake-shaped trap configuration, in which the underlying system of three-dimensional (3D) coupled Gross-Pitaevskii equations (GPEs) can be reduced to a two-dimensional (2D) form.

First, we consider the system with parameters corresponding to a nearly symmetric (with respect to the two components) ^{164}Dy-^{162}Dy mixture, where both components have equal dipole moments, thus supporting the balance between intra- and interspecies DDIs. In the absence of contact interactions, this mixture is miscible. Its miscibility-controlling parameter

is the ratio between scattering lengths of contact inter- and intraspecies repulsion, if it is added to the DDI. Next, we consider the setting with parameters of the asymmetric ^{168}Er-^{164}Dy mixture, with unequal dipole moments in the two species, which gives rise to imbalance of the inter- and intraspecies DDIs. This dipolar mixture produces immiscible states, in the absence of contact interactions. In this case too, mixing-demixing transition is controlled by the ratio of the scattering lengths of intra- and interspecies contact interactions, if they are present. The miscibility of these binary dipolar condensates determines vortex-lattice structures which can be created in them. We also briefly consider another binary system, in which only one component carries a dipole moment. The latter system favors the miscibility, in comparison with the symmetric and asymmetric mixtures of two dipolar components.

The paper is organized as follows. In Sec. II, we present the 2D mean-field model for the trapped two-component dipolar BEC under rotation, and we present the numerical methods used in this work. In Sec. III, we report numerical results for phase diagrams of vortex-lattice patterns, varying the strength of inter- and intraspecies contact interactions versus the rotation frequency, for different dipolar mixtures. Some analytical results, based on the Thomas-Fermi approximation for the immiscible system, are presented too. The paper is concluded by Sec. IV.

II. COUPLED DIPOLAR CONDENSATES UNDER ROTATION

The system of coupled GPEs for the binary condensate with the DDI, for the two-component wave functions $\Psi_{j=1,2} \equiv \Psi_j(\mathbf{r},t)$, can written as [23,24]

$$i\hbar \frac{\partial \Psi_j}{\partial t} = \left[-\frac{\hbar^2}{2m_j}\nabla^2 + V_j(\mathbf{r}) - \overline{\Omega}\hbar L_z + \sum_{k=1}^{2} G_{jk}N_k|\Psi_k|^2 \right. $$
$$\left. + \sum_{k=1}^{2} \frac{N_k}{4\pi} \int d^3\mathbf{r}' V_{jk}^{(d)}(\mathbf{r}-\mathbf{r}')|\Psi_k'|^2 \right]\Psi_j, \quad (1)$$

where $\Psi_k' \equiv \Psi_k(\mathbf{r}',t)$. The masses, the number of atoms, and the trapping potentials for the two species j are, respectively, given by m_j, N_j, and $V_j(\mathbf{r})$. Further, $V_{jk}^{(d)}(\mathbf{r}-\mathbf{r}')$ are the kernels of the DDI, $\overline{\Omega}$ is a common rotation frequency of both components, and $\hbar L_z = -i\hbar(x\partial/\partial y - y\partial/\partial x)$ is the angular-momentum operator. The strengths of the contact interactions are $G_{jk} \equiv (2\pi\hbar^2/m_{jk})a_{jk}$, where $m_{jk} = m_j m_k/(m_j + m_k)$ are the respective reduced masses, while a_{jk} are the corresponding intraspecies (a_{jj}) and interspecies (a_{12}) two-body scattering lengths. Trapping is provided by Harmonic-oscillator (HO) potentials with frequencies ω_j,

$$V_j(\mathbf{r}) = \frac{1}{2}m_j\omega_j^2(x^2+y^2+\lambda^2 z^2), \quad (2)$$

and the common aspect ratio λ for both components, such that the trap is spherically symmetric for $\lambda = 1$, cigar-shaped for $\lambda < 1$, and pancake-shaped for $\lambda > 1$. The DDI kernels in Eq. (1) correspond to the configuration with dipole moments polarized (by an external magnetic field) perpendicularly to

the (x,y) plane:

$$V_{ij}^{(d)}(\mathbf{r}-\mathbf{r}') = D_{ij}\frac{1-3\cos^2\theta}{|\mathbf{r}-\mathbf{r}'|^3}, \quad (3)$$

where θ is the angle between the polarized magnetic moments and $(\mathbf{r}-\mathbf{r}')$, and $D_{ij} \equiv \mu_0\mu_i\mu_j$, with the free-space permeability μ_0.

For the pancake-shaped dipolar BEC ($\lambda \gg 1$), we assume the usual factorization of the wave function into the ground state of the transverse HO trap and a 2D wave function:

$$\Psi_j(\mathbf{r},t) = \frac{1}{(\pi d_z^2)^{1/4}} \exp\left(-\frac{z^2}{2d_z^2}\right)\Phi_j(x,y,t), \quad (4)$$

where $d_z \equiv \sqrt{1/\lambda}$ is the trap's HO length [24–27]. To derive the effective coupled GPEs in 2D, we insert the ansatz (4) in Eq. (1), multiplying the equation by another power of the HO ground-state wave function, and perform integration over z. The coupled equations are cast in a dimensionless format by measuring the energy and the length in units of $\hbar\omega_1$ and $l \equiv \sqrt{\hbar/(m_1\omega_1)}$, respectively. By taking x and y variables in units of l ($x \to lx$ and $y \to ly$), the accordingly rescaled quantities are

$$\boldsymbol{\rho} \equiv x\hat{e}_1 + y\hat{e}_2, \quad \tau \equiv \omega_1 t,$$
$$g_{jk} \equiv \sqrt{2\pi\lambda}\frac{m_1}{m_{jk}}\frac{a_{jk}N_k}{l}, \quad \sigma \equiv \frac{m_2\omega_2^2}{m_1\omega_1^2},$$
$$a_{jj}^{(d)} \equiv \frac{D_{jj}}{12\pi}\frac{m_j}{m_1}\frac{1}{\hbar\omega_1 l^2}, \quad a_{12}^{(d)} = a_{21}^{(d)} = \frac{D_{12}}{12\pi}\frac{1}{\hbar\omega_1 l^2},$$
$$d_{jk} = \frac{N_j D_{jk}}{4\pi}\frac{1}{\hbar\omega_1 l^3} \quad (j,k=1,2), \quad (5)$$

with the corresponding 2D wave function for the components $j = 1$ and 2 given by

$$\psi_j(\boldsymbol{\rho},\tau) \equiv l\,\Phi_j(x,y,t). \quad (6)$$

In terms of this notation, for $\psi_j \equiv \psi_j(\boldsymbol{\rho},\tau)$ and $\psi_j' \equiv \psi_j(\boldsymbol{\rho}',\tau)$ the coupled GPEs in 2D take the form of

$$i\frac{\partial\psi_1}{\partial\tau} = \left[-\frac{1}{2}\nabla_\rho^2 + \frac{\rho^2}{2} - \Omega L_z + g_{11}|\psi_1|^2 + g_{12}|\psi_2|^2 \right.$$
$$\left. + \int d\boldsymbol{\rho}' V^{(d)}(\boldsymbol{\rho}-\boldsymbol{\rho}')(d_{11}|\psi_1'|^2 + d_{12}|\psi_2'|^2) \right]\psi_1,$$
$$i\frac{\partial\psi_2}{\partial\tau} = \left[-\frac{m_1}{2m_2}\nabla_\rho^2 + \frac{\sigma\rho^2}{2} - \Omega L_z + g_{22}|\psi_2|^2 + g_{21}|\psi_1|^2 \right.$$
$$\left. + \int d\boldsymbol{\rho}' V^{(d)}(\boldsymbol{\rho}-\boldsymbol{\rho}')(d_{22}|\psi_2'|^2 + d_{21}|\psi_1'|^2) \right]\psi_2,$$
$$(7)$$

where the common rotation frequency of the two components is written in terms of ω_1, such that $\Omega = \overline{\Omega}/\omega_1$.

In Eq. (7) the DD-interaction terms can be expressed by means of the convolution theorem,

$$\sum_{j=1}^{2}\int d\boldsymbol{\rho}' V^{(d)}(\boldsymbol{\rho}-\boldsymbol{\rho}')|\psi_j'|^2 = \mathcal{F}_{2D}^{-1}[\tilde{V}^{(d)}(k_\rho)\tilde{n}_j(\mathbf{k}_\rho,\tau)], \quad (8)$$

where $\mathcal{F}_{2D}^{-1}$ is the inverse 2D Fourier-transform operator, with $k_\rho \equiv \sqrt{k_x^2 + k_y^2}$,

$$\tilde{n}_j(\mathbf{k}_\rho, \tau) = \int d\boldsymbol{\rho} \, e^{i\mathbf{k}_\rho \cdot \boldsymbol{\rho}} |\psi_j|^2, \tilde{n}_j(k_z) = e^{-k_z^2 d_z^2/4}, \quad (9)$$

and

$$\tilde{V}^{(d)}(k_\rho) \equiv \frac{1}{2\pi} \int_{-\infty}^{\infty} dk_z \left(\frac{3k_z^2}{\mathbf{k}^2} - 1 \right) |\tilde{n}_j(k_z)|^2$$

$$= \frac{1}{\sqrt{2\pi} d_z} \left\{ 2 - \frac{3\sqrt{\pi}}{\sqrt{2}} k_\rho d_z \exp\left(\frac{k_\rho^2 d_z^2}{2} \right) \right.$$

$$\left. \times \left[1 - \text{erf}\left(\frac{k_\rho d_z}{\sqrt{2}} \right) \right] \right\}. \quad (10)$$

For the numerical solution of Eq. (7), we employed the split-step Crank-Nicolson method, as in Refs. [27–29], combined with the standard method for evaluating DDI integrals in the momentum space [23,27]. To look for stable solutions, numerical simulations were carried out in imaginary time on a grid with 512 points in the x and y directions, spatial steps $\Delta x = \Delta y = 0.05$, and time step $\Delta t = 0.0005$. Both component wave functions are renormalized to 1, $\int d\boldsymbol{\rho} |\psi_j|^2 = 1$, at each time step.

To calculate stationary vortex states, Eq. (7) was solved with different initial conditions. From the tests, we chose the following suitable initial conditions in the form of a combination of angular harmonics [30],

$$\psi_j(\boldsymbol{\rho}, 0) = \sum_{m=0}^{L} \frac{(x + iy)^m e^{(-\rho^2/2)}}{\sqrt{\pi(L+1)m!}} \exp(2\pi i \mathcal{R}_m), \quad (11)$$

where $\mathcal{R}_m$ is a randomly generated number distributed uniformly between 0 and 1, with the arbitrary integer value for L that we have consider up to $L = 40$. In addition, we checked the convergence of the solutions with inputs as considered in Ref. [31].

For the parameters, we follow the ones used in a previous study on miscibility in coupled dipolar condensates, given in Ref. [22], for atomic mixtures of erbium (^{168}Er) and dysprosium (^{162,164}Dy) isotopes. In terms of the Bohr magneton μ_B, the corresponding dipole moments are, respectively, $\mu = 7\mu_B$ and $\mu = 10\mu_B$. In the harmonic axial traps, defined in Eq. (2), the assumed angular frequencies confining each species are such that $\omega_j = 2\pi \times 60\,\text{s}^{-1}$ for the ^{168}Er and $\omega_j = 2\pi \times 61$ s^{-1} for the ^{162,164}Dy, such that σ defined in Eq. (5) is close to 1. The time and space units are such that $1/\omega_1 = 2.65$ ms and $l = 1\,\mu\text{m} (= 10^4\,\text{Å} = 1.89 \times 10^4\,a_0)$. As found appropriate for experimentally realistic settings, in all the following analysis and results we are taking a pancake-shaped trap, with an aspect ratio of $\lambda = 20$, and we fix the number of atoms to be equal for both species with $N_1 = N_2 = 10^4$. The contact and dipole-dipole interactions, expressed in terms of the Bohr radius a_0, are varied by considering several conditions of interest in view of miscibility properties of the binary mixtures. In particular, considering the corresponding dipole moments, the strengths of the DDI are given as $a_{11}^{(d)} = a_{22}^{(d)} = 131\,a_0$ and $a_{12}^{(d)} = a_{21}^{(d)} = 131\,a_0$, for the ^{164}Dy-^{162}Dy mixture; and $a_{11}^{(d)} = 66\,a_0$, $a_{22}^{(d)} = 131\,a_0$, and $a_{12}^{(d)} = a_{21}^{(d)} = 94\,a_0$, for the

^{168}Er-^{164}Dy mixture. Further, in order to explore various families of vortex patterns, we varied the rotation frequency Ω.

As transitions between vortex-lattice structures are determined by the miscibility, it is appropriate to consider a parameter to measure the overlapping between densities of the components, such as the one defined in Ref. [22]:

$$\eta = \int |\psi_1||\psi_2| d\boldsymbol{\rho} \equiv \int \sqrt{|\psi_1|^2|\psi_2|^2} d\boldsymbol{\rho}. \quad (12)$$

As ψ_1 and ψ_2 are both normalized to 1, a complete overlap between the species has $\eta = 1$, with indications of partial overlapping for smaller values of η. Results reported in the following are suggesting that values of $\eta \lesssim 0.5$ correspond to almost clear demixing, as the maxima for the densities are located at well-separated points. In the interval of $0.5 < \eta < 0.8$, the system may be categorized as partially miscible, as one can notice that the peaks of the densities are approaching each other. The density maxima are nearly overlapping for $\eta \gtrsim 0.8$, such that we can identify the system as a miscible one. The applicability of these definitions was checked for all settings considered in this work.

III. RESULTS

The numerical results presented in this section are organized in four subsections, considering possible nonlinear effects due to the interplay of the contact and dipolar interactions. We start by considering a pure-dipolar case (Sec. III A). Next, in other subsections, we vary the strength of contact interactions, considering a nearly symmetric dysprosium-dysprosium mixture (Sec.III B); a nonsymmetric erbium-dysprosium mixture (Sec. III C); and, finally, a mixture of dipolar and nondipolar species (Sec. III D). As mentioned above, the harmonic-trap aspect ratio and the number of atoms in both components are fixed, respectively, to $\lambda = 20$ and $N_1 = N_2 = 10^4$, which are adjusted to the previous studies of the stability and miscibility of binary dipolar condensates [22]. All the following results are produced with parameters of the contact and dipolar interactions given in units of the Bohr radius a_0. Adopting the length unit as $l = 1.89 \times 10^4\,a_0$, the coordinates and densities are presented as dimensionless quantities.

A. Vortex structures in dipolar binary condensates in the absence of contact interactions

To illustrate the miscible or immiscible states in the absence of the contact interactions ($a_{jk} = 0$, for $j,k = 1,2$), we display stable solutions for densities and phases, corresponding to the dipolar mixtures ^{164}Dy-^{162}Dy (Fig. 1) and ^{168}Er-^{164}Dy (Fig. 2). In both cases, we apply the same rotation frequency $\Omega = 0.6$ and aspect ratio $\lambda = 20$. As defined by Eq. (12), the miscibility parameter is much larger for the ^{164}Dy-^{162}Dy BEC mixture, $\eta = 0.81$, corresponding to an almost completely miscible state. On the other hand, for the ^{168}Er-^{164}Dy system, we have a smaller value of $\eta = 0.19$, implying an almost immiscible composition. The predicted lattice patterns for the vortices, considering these miscible and immiscible binary dipolar condensates, are presented in Figs. 1 and 2, respectively. The patterns may be naturally classified as squared- to
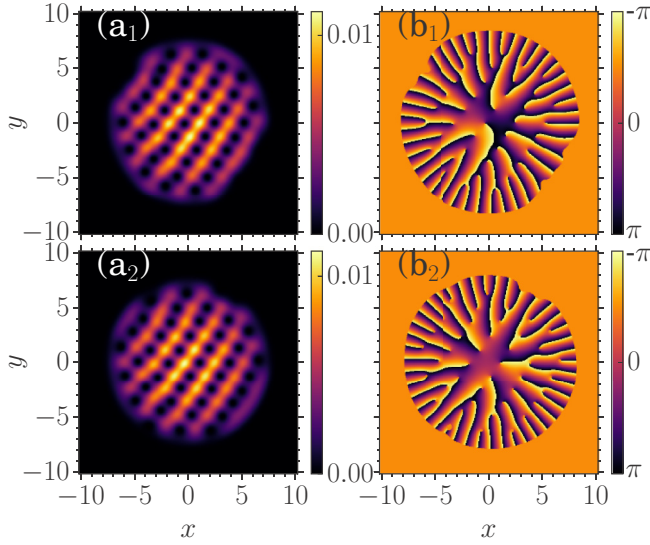
FIG. 1. The 2D density (left panels) and phase (right panels) patterns for the miscible ^{164}Dy-^{162}Dy system with no-contact interactions are shown by the upper (component $j = 1$) and lower (component $j = 2$) panels. The parameters are $a_{jk} = 0$, $a_{jk}^{(d)} = 131a_0$, $\Omega = 0.6$, $\lambda = 20$, and $N_j = 10^4$ ($j,k = 1,2$).

striped-shaped lattices in the more miscible case, and as having a finite segment of a hexagonal lattice in one component, surrounded by a ring in the other component in the immiscible mixture.

B. The nearly symmetric ^{164}Dy-^{162}Dy mixture under the action of contact interactions

To drive the mixing-demixing transition in the dipolar mixtures in the presence of contact interactions, we use
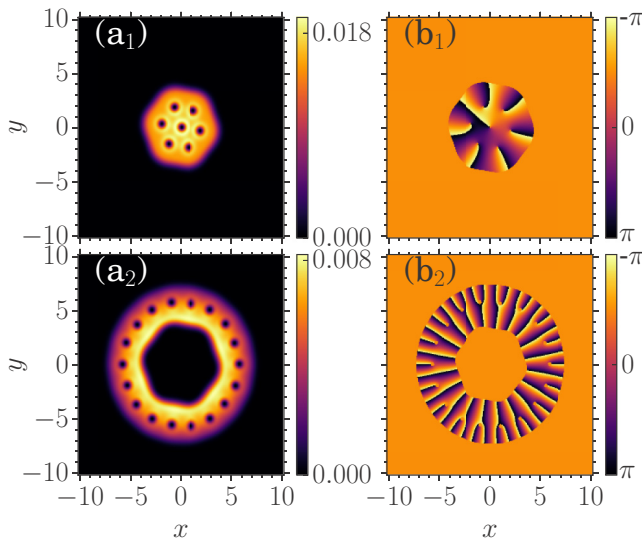

FIG. 2. The 2D density (left panels) and phase (right panels) patterns for the immiscible ^{168}Er-^{164}Dy system with no-contact interactions are shown by the upper (component $j = 1$) and lower (component $j = 2$) frames. The parameters are $a_{jk} = 0$, $a_{11}^{(d)} = 66\,a_0$, $a_{22}^{(d)} = 131\,a_0$, $a_{12}^{(d)} = a_{21}^{(d)} = 94\,a_0$, $\Omega = 0.6$, $\lambda = 20$, and $N_j = 10^4$ ($j,k = 1,2$).
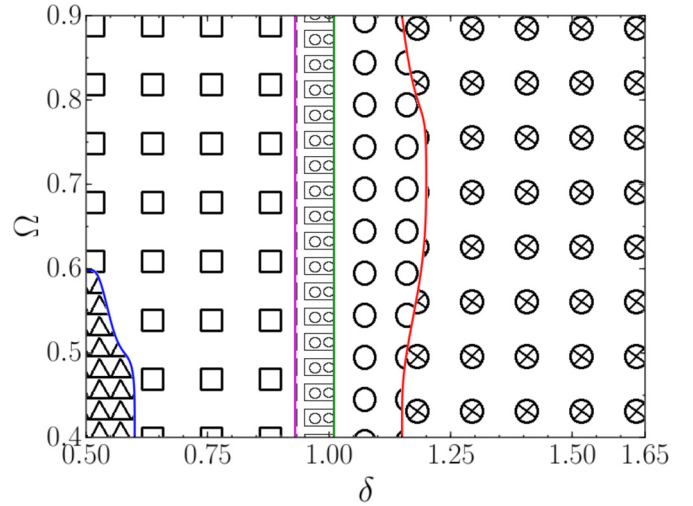

FIG. 3. The phase diagram of vortex patterns in the plane defined by the angular velocity Ω and the ratio between inter- and intraspecies scattering length $\delta \equiv a_{12}/a_{11}$ for the ^{164}Dy-^{162}Dy mixture. The symbols for the observed patterns are as follows: triangles for triangular lattices, squares for squared lattices, double circles inside a rectangle for rectangular or double-core vortices, circles for striped vortices, and crossed circles for domain walls. Typical examples are displayed in Figs. 4–6.

the scattering lengths as tuning parameters. For that, the intraspecies scattering lengths are assumed to be equal, $a_{11} = a_{22}$, with the ratio between inter- and intraspecies scattering lengths being defined by

$$\delta = \frac{a_{12}}{a_{11}}. \tag{13}$$

Therefore, stable vortex states are explored by varying this ratio δ and the rotation frequency Ω, which is given in units of the trap frequency ω_1. We consider this parameter for the rotation in the interval $0.4 < \Omega < 0.9$, as this interval adequately represents various types of vortex patterns which the system can generate. In this work we restrict the analysis to the case of equal intraspecies scattering lengths, $a_{11} = a_{22}$, as effects produced by the variation of the interspecies interaction/intraspecies interaction ratio δ, defined by Eq. (13), are essentially stronger (and more interesting) than what may be controlled by the variation of a_{22}/a_{11}. Systematic analysis of the latter effects may be considered separately, to keep the length of the present paper within reasonable limits.

A commonly known result for spatially uniform states in the absence of DDIs is that the miscibility and immiscibility take place at $\delta < 1$ and $\delta > 1$, respectively [32]. Stable vortex structures found in different domains of the (δ, Ω) plane for parameters of the ^{164}Dy-^{162}Dy mixture (assuming that a_{12} can be adjusted by means of the Feshbach resonance) are summarized in the phase diagram exhibited in Fig. 3, with typical examples of different stable patterns shown in Fig. 4 for $\Omega = 0.4$.

In the well-miscible state, at $\delta < 0.9$, triangular- and square-shaped vortex lattices are found as stable patterns. With the onset of immiscibility, positions of vortices in one component shift with respect to the other, which leads to a transition
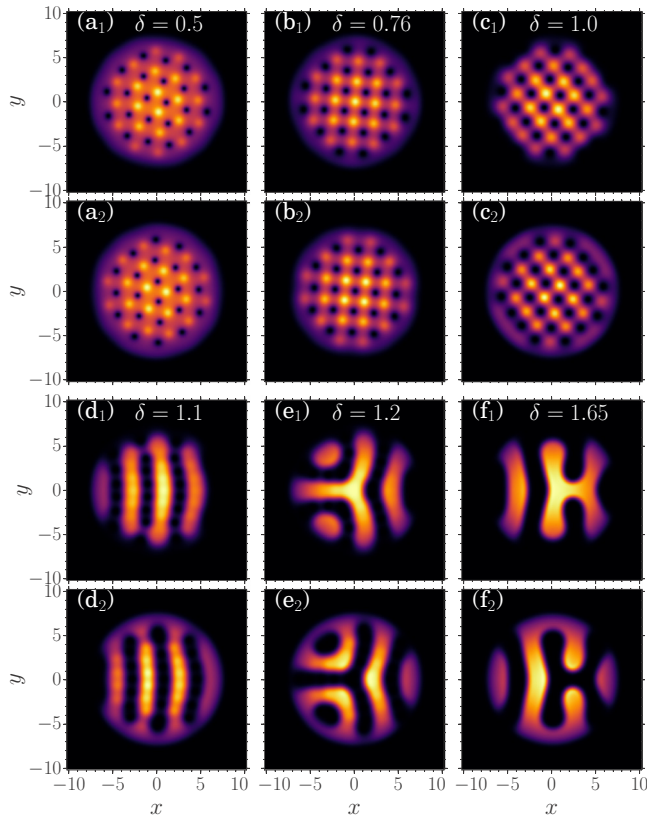
FIG. 4. The 2D component densities, $|\psi_j|^2$ [(a$_j$) to (f$_j$), with $j = 1,2$], for the ^{164}Dy-^{162}Dy mixture in different patterns of stable vortices, following the phase diagram in Fig. 3 for δ varying from 0.5 to 1.65, as indicated. The lattices are triangular (a$_{j=1,2}$), squared (b$_{j=1,2}$), rectangular (c$_{j=1,2}$), striped (d$_{j=1,2}$), and with domain walls [(e$_{j=1,2}$) and (f$_{1,2}$)]. Other parameters are $N_{j=1,2} = 10^4, \lambda = 20, a_{12} = 50\, a_0$, and $\Omega = 0.4$.

in the respective lattice structure. Namely, at $0.9 < \delta < 1.02$ the square-shaped lattice is transformed into the rectangle one, as the vortices in each component tend to get closer and form stripes. Therefore, in this regime, the system produces rectangular and double-core vortices. Thus, in the immiscible

state at $\delta > 1$, we observe vortex stripes and also patterns that may be called domain walls [see the panels (f$_{1,2}$) of Fig. 4]. Actually, the phase diagram displayed in Fig. 3 is similar to its counterpart produced for nondipolar BEC in Ref. [6], as well as to the phase diagram for nondipolar condensates produced in Ref. [5] on the basis of the lowest-Landau-level approximation. This similarity is explained by the fact that, in the nearly symmetric ^{164}Dy-^{162}Dy binary system, with equal dipole moments of both species, effects of equal intra- and interspecies DDIs on the miscibility almost cancel.

In Figs. 4 and 5, by considering the ^{164}Dy-^{162}Dy mixture, we display typical density plots for vortex lattices with different patterns, such as triangular, squared, rectangular, stripes, and domain walls, according to values of δ, which may correspond to miscible or immiscible cases. In Fig. 4, with $\Omega = 0.4$, one can observe that the stripe pattern forms overlapping lines of vortices in both components. In the double-core structure, the vortex lattice in the second component is formed by pairs of vortices with the same circulation and vortices in the first component surrounded by those pairs. In the strongly phase-separated regime, at $\delta > 1$, vortices in one component are located very closely, merging into the domain wall, with the walls in the two components being mutually interlaced. In Fig. 5 we consider the same parameters as in Fig. 4, except that the rotation frequency is changed to $\Omega = 0.6$, in order to verify how the lattice shapes are being affected by Ω. In Fig. 6, further examples for the ^{164}Dy-^{162}Dy mixture are displayed by striped vortices and domain walls, with $\delta > 1$, by considering the large value $\Omega = 0.8$ of the rotation frequency.

The Thomas-Fermi (TF) density distribution for the overlapping binary BECs subject to the solid rotation was verified in Ref. [6] to be a good approximation to the corresponding total density distribution $\boldsymbol{n}_T = |\psi_1|^2 + |\psi_2|^2$. Due to the repulsion between the species, a vortex in one component corresponds to a density peak in the other, and vice versa. In the present work, we have confirmed that the TF expression, given in Ref. [6], which can also be derived by following the lines of Ref. [33], $\boldsymbol{n}_{\text{TF}}(\rho) = 2\sqrt{\alpha/\pi} - \alpha\rho^2$, holds also for the parameter regimes we are considering in the presence of DDIs, with $\alpha \equiv (1 - \Omega^2)/(g_{11} + d_{11} + g_{12} + d_{12})$. The agreement was confirmed for different miscible dipolar BEC mixtures.
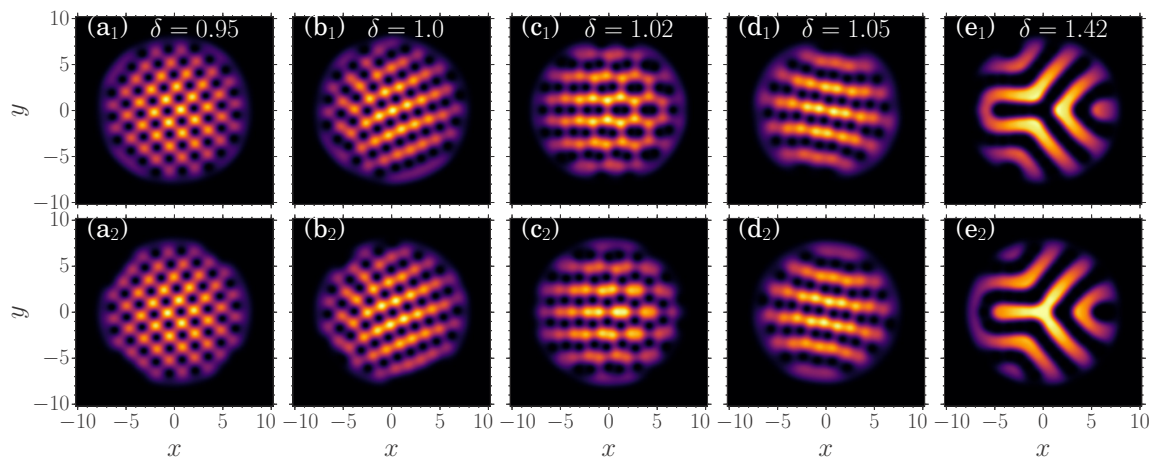

FIG. 5. The 2D component densities, with the same parameters as in Fig. 4, by changing the rotation frequency to $\Omega = 0.6$.
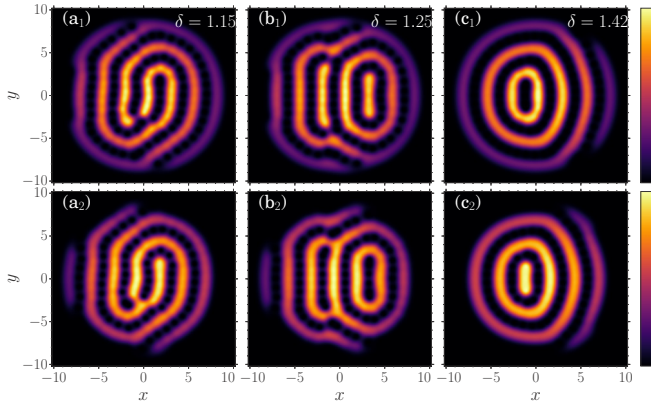
FIG. 6. The 2D component densities, with the same parameters as in Fig. 4, by changing the rotation frequency to $\Omega = 0.8$. The color bar on the right specifies variation of the density from 0 (darker) to 0.01 (lighter).

In Fig. 7, the miscible structure of the binary system is illustrated by the dependence of parameter η, defined by Eq. (12), on the ratio between inter- and intrascattering lengths as defined by Eq. (13), for different values of Ω.

C. The asymmetric ^{168}Er-^{164}Dy mixture under the action of contact interactions

The phase diagram of vortex patterns for parameters corresponding to the ^{168}Er-^{164}Dy mixture is displayed in Fig. 8. Recall that, in the absence of contact interactions, this system is immiscible, as shown above in Fig. 2. However, imbalanced inter- and intraspecies contact interactions can impose miscibility in this setting. The phase diagram of the asymmetric system is drastically different from that for its symmetric ^{164}Dy-^{162}Dy counterpart, due to the miscibility of the latter in the absence of contact interactions (cf. Fig. 3). Note
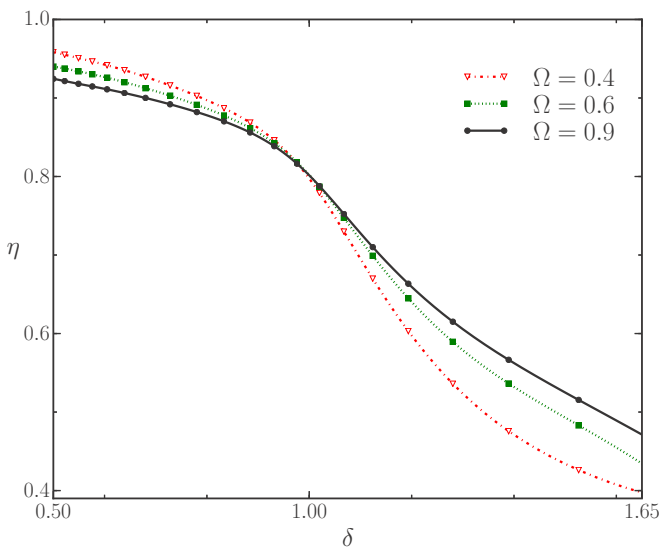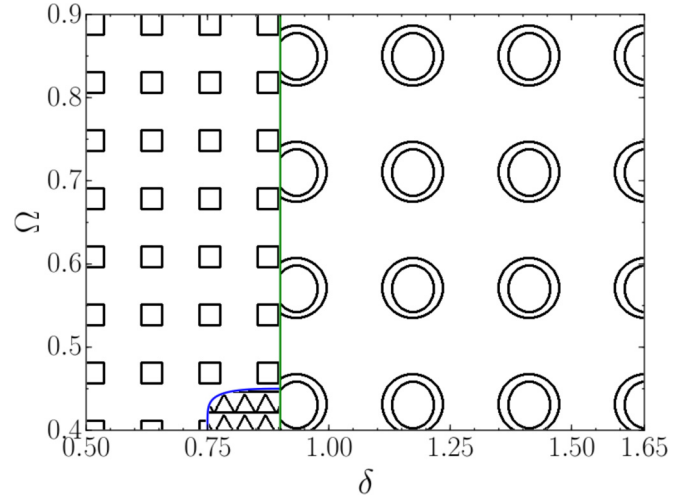

FIG. 8. The phase diagram of vortex patterns in the plane defined by δ and the rotation frequency Ω plane, for the asymmetric ^{168}Er-^{164}Dy mixture. The symbols for the observed lattice patterns are as follows: triangles for triangular-shaped, squares for squared-shaped, and concentric circles for circular lattices.

that, while the immiscibility in nondipolar binary condensates takes place at $\delta > 1$, in the ^{168}Er-^{164}Dy system complete immiscibility commences from $\delta = 0.9$. The shift to $\delta < 1$ is induced by the imbalance of the DDI.

In the case of immiscible states for the ^{168}Er-^{164}Dy system at $\delta > 0.9$, only circular-shaped lattices are established. In both the miscible and immiscible states, the squared- and circular-shaped lattices are shown in Figs. 9 and 10. Due to immiscibility, the first component is surrounded by the second component, (cf. Fig. 2 which displays a similar arrangement in the immiscible system of the ^{168}Er-^{164}Dy type). In such a phase-segregated mixture, vortices in the second component are arranged into a circular lattice. A similar situation may also occur in asymmetric nondipolar systems with $a_{11} \neq a_{22}$ and $a_{12} = \sqrt{a_{11}a_{22}}$, when unequal intraspecies interactions may balance the interspecies repulsion [8].
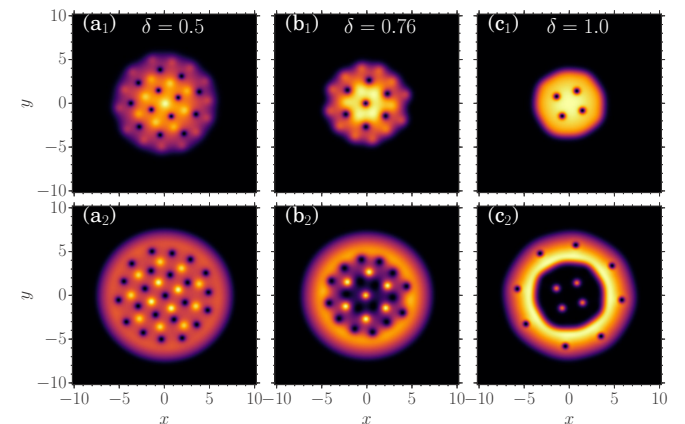

FIG. 7. Miscibility parameter η [Eq. (12)] is plotted in terms of δ for the ^{164}Dy-^{162}Dy mixture at different values of the rotation frequency Ω.

FIG. 9. Similar to Fig. 4, for the ^{168}Er-^{164}Dy mixture, we have the 2D densities $|\psi_j|^2$ for several values of δ. As in Fig. 4, we have the rotation frequency $\Omega = 0.4$, with the other parameters given by $N_{j=1,2} = 10^4$, $\lambda = 20$, and $a_{12} = 50\,a_0$.
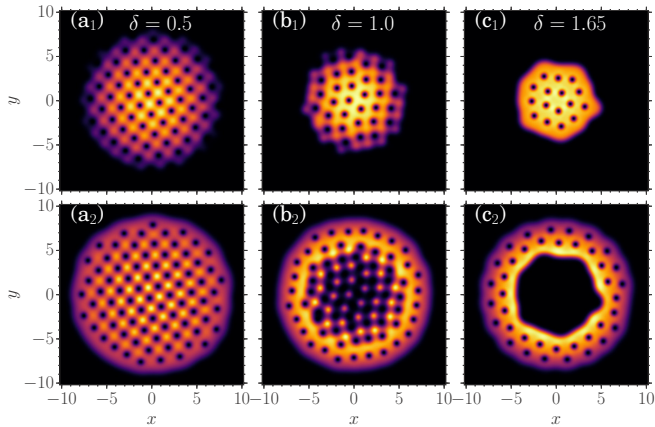
FIG. 10. The same as in Fig. 9, with the rotation frequency changed to $\Omega = 0.8$.

In Fig. 11, where the miscibility parameter η is shown as a function of the scattering-length ratio δ [see Eq. (13)], one can verify that the behavior obtained for the asymmetric ^{168}Er-^{164}Dy mixture is quite different from that of the nearly symmetric ^{164}Dy-^{162}Dy mixture shown in Fig. 7. By considering the same scattering lengths for both species ($\delta \approx 1$) we see that the large miscibility of the dipolar ^{164}Dy-^{162}Dy mixture (with $\eta \approx 0.8$) is not too much affected by the rotation. However, in the same condition ($\delta \approx 1$), the miscibility of the dipolar asymmetric ^{168}Er-^{164}Dy mixture is strongly affected by the rotation: faster rotation increases the miscibility of the mixture. As a general trend, for a large range of values for δ, faster rotations tend to enhance mixing (increasing η) of the asymmetric dipolar mixture. This behavior is reversed only for $\delta \gtrsim 1.5$. When the interspecies scattering length a_{12} is about $1.5\, a_{11}$ or larger, the miscibility decreases for larger rotations. In Table 1, we can better verify the dependence of the
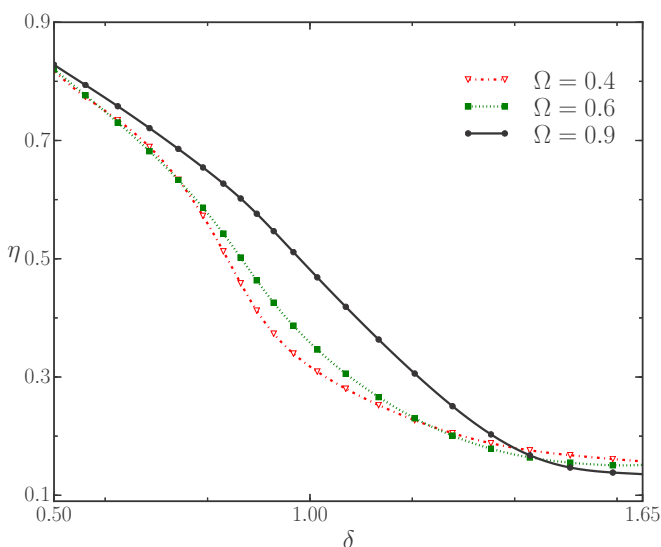

FIG. 11. The miscibility parameter η [Eq. (12)] as a function of $\delta = a_{12}/a_{11}$ (with $a_{11} = a_{22}$ and $a_{12} = 50\, a_0$) for the ^{168}Er-^{164}Dy mixture is represented for three different values of the rotation frequency Ω as indicated.

TABLE I. Miscibility parameter η [Eq. (12)] as a function of the interspecies and intraspecies scattering-length ratio, $\delta \equiv a_{12}/a_{11}$, at different values of the rotation frequency Ω for the mixtures considered in the paper. For the sake of comparison, in our analysis a mixture with dipolar and nondipolar species, ^{164}Dy-^{85}Rb, is also included.

δ	Ω	η ^{164}Dy-^{162}Dy	η ^{168}Er-^{164}Dy	η ^{164}Dy-^{85}Rb
0.5	0.0	1.0	0.86	0.93
	0.4	0.95	0.81	0.83
	0.9	0.92	0.82	0.82
1.0	0.0	0.99	0.32	0.73
	0.4	0.83	0.30	0.69
	0.9	0.83	0.48	0.69
1.5	0.0	0.23	0.17	0.59
	0.4	0.39	0.15	0.53
	0.9	0.46	0.13	0.54

miscibility on changes of the rotation parameter, for different values of δ, considering the two mixtures we are studying, as well as a case where one of the species is nondipolar, which is discussed in the following subsection.

D. The mixture of dipolar and nondipolar species

In this subsection we briefly comment on the coupled ^{164}Dy-^{85}Rb mixture, where the magnetic moment of the second species (^{85}Rb) is negligible. This type of mixture was discussed in Ref. [34], where half-quantum vortex chains were reported, such that here we just include our corresponding results in Table I for the sake of comparison with the results we have obtained for the symmetric and asymmetric dipolar mixtures. We summarize in Table I our results for the dependence of the miscibility parameter η on the relevant control parameters which are considered in the present work, i.e., the scattering-length ratio δ [Eq. (13)] and the rotation frequency Ω.

As a general remark, it is observed from the two-component mixture of the ^{164}Dy-^{85}Rb type that the absence of the dipole-dipole repulsion between the two components tends to make the mixture less miscible in the presence of the rotation. When there is no rotation, the strong role of the ratio between the scattering lengths is clear, with the miscibility decreasing significantly for larger values of δ. This trend is attenuated by increasing the rotation of the coupled systems, as faster rotations tend to enhance mixing. Another remark is that the asymmetric dipolar mixture, ^{168}Er-^{164}Dy, is always less miscible than the others two mixtures.

IV. SUMMARY AND CONCLUSION

Stimulated by the current interest from experiments with dipolar BEC mixtures, we have developed a detailed theoretical analysis for two corotating mixtures: one nearly symmetric (corresponding to parameters of the ^{164}Dy-^{162}Dy system), and one asymmetric, which represents the ^{168}Er-^{164}Dy mixture. The dynamics of the mixtures is described by the effectively 2D system of coupled GPEs (Gross-Pitaevskii equations), which was derived from the full 3D system under the assumption of

strong confinement in the transverse direction. For that, we consider pancake-type condensates with the aspect ratio given by $\lambda = 20$. The coupled equations include both the repulsive dipole-dipole interactions and repulsive contact interactions, with our results being presented in two-dimensional density plots, complemented by phase diagram analysis relatint the two main parameters found for the miscibility of the species: the rotation angular parameter Ω and the ratio between scattering lengths for the inter- and intraspecies contact interactions, given by δ. The phase diagrams display stability regions for several basic types of binary vortex lattices. In the absence of the contact interactions, the symmetric system is miscible, while the asymmetric one is not. The addition of contact interactions can change significantly the situation. For the symmetric mixture, ^{164}Dy-^{162}Dy, the phase diagram is similar to those recently found for binary nondipolar condensates. It includes regions supporting the following vortex lattices: triangular, square-shaped, rectangular-shaped, double core, striped, and with domain walls. The phase diagram for the asymmetric mixture, ^{168}Er-^{164}Dy, includes triangular, square-shaped, and circular lattices.

To understand the origin of the observed vortex patterns, it is relevant to recall a previous work [21], where vortices in a dipolar-nondipolar mixture were considered. It was found that the role of the dipolar component is to create vortices when the long-range dipolar interactions dominate over the contact nonlinearity. Following the pattern, we start the presentation of our results by considering pure dipolar mixtures, with both components involved in the dipolar interactions. In this case, the long-range interactions give rise to two distinct kinds of vortex patterns, displayed in Figs. 1 and 2, the selection of a particular one being mainly determined by the miscibility or the immiscibility of the two-component system. The miscible system favors the square-shaped or striped lattices, whereas the immiscibility tends to establish a hexagonal lattice in one component, surrounded by a ring-shaped structure in the other. It is concluded from the consideration of the settings which include contact interactions that, in addition to the rotation frequency, the shape of the observed patterns is strongly affected by the (im)miscibility of the coupled system, which may be effectively shifted by the contribution from the contact interactions.

By summarizing the net effect of rotation, as well as contact interactions, in the miscibility of dipolar coupled systems, complementing the analysis presented in the Figs. 7 and 11, we include Table I, for three values of the rotation parameter Ω and three values of the scattering-ratio parameter δ. In this table, for the sake of comparison with the dipolar systems which we have studied, we also add results obtained for a nondipolar coupled system, the ^{164}Dy-^{85}Rb mixture, where the magnetic moment of the second species (^{85}Rb) is negligible. As can be seen, by increasing the rotation, the coupled system becomes less miscible. The strong role of the ratio between the scattering lengths δ for the miscibility can be clearly verified from the results given in the table, with the parameter η decreasing significantly as we increase this ratio. The general trend of the rotation is to attenuate such an effect by increasing the rotation of the coupled systems.

To finally summarize, we have presented results on vortex-lattice structures expected to be of general interest in studies with dipolar mixtures. By considering particular dipolar mixtures, in specific pancake-type geometry, we are contemplating dipolar BEC systems in stable configurations, which are under active investigations in cold-atom laboratories, with promising potential realization. Possible extensions of the present work on rotating binary condensates could be by including spin-orbit coupling effects, following analysis also studied in Ref. [35]. Another challenging generalization can be by studying spatially anisotropic quasi-2D configurations, with the magnetic dipoles oriented not perpendicularly to the system's plane, but rather in the surface, considering that bright solitons were verified in such a configuration [36].

ACKNOWLEDGMENTS

[1] A. L. Fetter, Ann. Phys. **70**, 67 (1972); F. Dalfovo, S. Giorgini, L. P. Pitaevskii, and S. Stringari, Rev. Mod. Phys. **71**, 463 (1999); A. L. Fetter and A. A. Svidzinsky, J. Phys.: Condens. Matter **13**, R135 (2001); P. G. Kevrekidis, R. Carretero-González, D. J. Frantzeskakis, and I. G. Kevrekidis, Mod. Phys. Lett. B **18**, 1481 (2004); A. L. Fetter, Rev. Mod. Phys. **81**, 647 (2009); H. Saarikoski, S. M. Reimann, A. Harju, and M. Manninen, *ibid.* **82**, 2785 (2010); S. Serafini, L. Galantucci, E. Iseni, T. Bienaimé, R. N. Bisset, C. F. Barenghi, F. Dalfovo, G. Lamporesi, and G. Ferrari, Phys. Rev. X **7**, 021031 (2017).

[2] K. W. Madison, F. Chevy, W. Wohlleben, and J. Dalibard, Phys. Rev. Lett. **84**, 806 (2000); B. P. Anderson, P. C. Haljan, C. A. Regal, D. L. Feder, L. A. Collins, C. W. Clark, and E. A.

Cornell, *ibid.* **86**, 2926 (2001); A. E. Leanhardt, A. Görlitz, A. P. Chikkatur, D. Kielpinski, Y. Shin, D. E. Pritchard, and W. Ketterle, *ibid.* **89**, 190403 (2002); E. A. L. Henn, J. A. Seman, G. Roati, K. M. F. Magalhães, and V. S. Bagnato, *ibid.* **103**, 045301 (2009).

[3] A. E. Leanhardt, Y. Shin, D. Kielpinski, D. E. Pritchard, and W. Ketterle, Phys. Rev. Lett. **90**, 140403 (2003).

[4] A. M. Martin, N. G. Marchant, D. H. J. O'Dell, and N. G. Parker, J. Phys.: Condens. Matter **29**, 103004 (2017).

[5] E. J. Mueller and T. L. Ho, Phys. Rev. Lett. **88**, 180403 (2002).

[6] K. Kasamatsu, M. Tsubota, and M. Ueda, Phys. Rev. Lett. **91**, 150406 (2003); K. Kasamatsu and M. Tsubota, Phys. Rev. A **79**, 023606 (2009).

[7] N. Ghazanfari, A. Keles, and M. Ö. Oktel, Phys. Rev. A **89**, 025601 (2014).

[8] P. Mason and A. Aftalion, Phys. Rev. A **84**, 033611 (2011).

[9] I. Ferrier-Barbut, H. Kadau, M. Schmitt, M. Wenzel, and T. Pfau, Phys. Rev. Lett. **116**, 215301 (2016).

[10] M. Schmitt, M. Wenzel, F. Böttcher, I. Ferrier-Barbut, and T. Pfau, Nature (London) **539**, 259 (2016).

[11] L. Chomaz, S. Baier, D. Petter, M. J. Mark, F. Wächtler, L. Santos, and F. Ferlaino, Phys. Rev. X **6**, 041039 (2016).

[12] D. S. Petrov, Phys. Rev. Lett. **115**, 155302 (2015).

[13] D. S. Petrov and G. E. Astrakharchik, Phys. Rev. Lett. **117**, 100401 (2016).

[14] Y. Li, Z. Luo, Y. Liu, Z. Chen, C. Huang, S. Fu, H. Tan, and B. A. Malomed, New J. Phys. **19**, 113043 (2017).

[15] C. R. Cabrera, L. Tanzi, J. Sanz, B. Naylor, P. Thomas, P. Cheiney, and L. Tarruell, Science **358**, eaao5686 (2017).

[16] G. Semeghini, G. Ferioli, L. Masi, C. Mazzinghi, L. Wolswijk, F. Minardi, M. Modugno, G. Modugno, M. Inguscio, and M. Fattori, arXiv:1710.10890v1 [cond-mat.quant-gas].

[17] P. Cheiney, C. R. Cabrera, J. Sanz, B. Naylor, L. Tanzi, and L. Tarruell, arXiv:1710.11079v1 [cond-mat.quant-gas].

[18] S. Yi and H. Pu, Phys. Rev. A **73**, 061602(R) (2006).

[19] F. Malet, T. Kristensen, S. M. Reimann, and G. M. Kavoulakis, Phys. Rev. A **83**, 033628 (2011).

[20] R. K. Kumar and P. Muruganandam, J. Phys. B: At. Mol. Opt. Phys. **45**, 215301 (2012); Eur. Phys. J. D **68**, 289 (2014); R. K. Kumar, T. Sriraman, H. Fabrelli, P. Muruganandam, and A. Gammal, J. Phys. B: At. Mol. Opt. Phys. **49**, 155301 (2016).

[21] Y. Zhao, J. An, and C. D. Gong, Phys. Rev. A **87**, 013605 (2013).

[22] R. K. Kumar, P. Muruganandam, L. Tomio, and A. Gammal, J. Phys. Commun. **1**, 035012 (2017).

[23] K. Góral and L. Santos, Phys. Rev. A **66**, 023613 (2002).

[24] R. M. Wilson, C. Ticknor, J. L. Bohn, and E. Timmermans, Phys. Rev. A **86**, 033606 (2012).

[25] L. Salasnich, Laser Phys. **12**, 198 (2002); L. Salasnich, A. Parola, and L. Reatto, Phys. Rev. A **65**, 043614 (2002).

[26] L. Salasnich and B. A. Malomed, Phys. Rev. A **79**, 053620 (2009).

[27] R. K. Kumar, L. E. Young-S, D. Vudragović, A. Balaž, P. Muruganandam, and S. K. Adhikari, Comput. Phys. Commun. **195**, 117 (2015).

[28] A. Gammal, T. Frederico, and L. Tomio, Phys. Rev. A **64**, 055602 (2001); A. Gammal, L. Tomio, and T. Frederico, *ibid.* **66**, 043619 (2002); M. Brtka, A. Gammal, and L. Tomio, Phys. Lett. A **359**, 339 (2006).

[29] P. Muruganandam and S. K. Adhikari, Comp. Phys. Commun. **180**, 1888 (2009); D. Vudragović, I. Vidanović, A. Balaž, P. Muruganandam, and S. K. Adhikari, *ibid.* **183**, 2021 (2012).

[30] D. A. Butts and D. S. Rokhsar, Nature (London) **397**, 327 (1998).

[31] W. Bao, H. Wang, and P. A. Markowich, Comm. Math. Sci. **3**, 57 (2005); B. W. Jeng, Y. S. Wang, and C. S. Chien, Comput. Phys. Commun. **184**, 493 (2013).

[32] V. P. Mineev, Zh. Eksp. Teor. Fiz. **67**, 263 (1974) [Sov. Phys.-JETP **40**, 132 (1975)].

[33] Y. Li, J. Liu, W. Pang, and B. A. Malomed, Phys. Rev. A **88**, 053630 (2013).

[34] W. E. Shirley, B. M. Anderson, C. W. Clark, and R. M. Wilson, Phys. Rev. Lett. **113**, 165301 (2014).

[35] X.-Q. Xu and J. H. Han, Phys. Rev. Lett. **107**, 200401 (2011); T. Kawakami, T. Mizushima, and K. Machida, Phys. Rev. A **84**, 011607(R) (2011); J. Radić, T. A. Sedrakyan, I. B. Spielman, and V. Galitski, *ibid.* **84**, 063604 (2011); X.-F. Zhou, J. Zhou, and C. Wu, *ibid.* **84**, 063624 (2011); Z. F. Xu, Y. Kawaguchi, L. You, and M. Ueda, *ibid.* **86**, 033628 (2012); E. Ruokokoski, J. A. M. Huhtamäki, and M. Möttönen, *ibid.* **86**, 051607(R) (2012); B. Ramachandhran, B. Opanchuk, X.-J. Liu, H. Pu, P. D. Drummond, and H. Hu, *ibid.* **85**, 023606 (2012); H. Sakaguchi and B. Li, *ibid.* **87**, 015602 (2013).

[36] I. Tikhonenkov, B. A. Malomed, and A. Vardi, Phys. Rev. Lett. **100**, 090406 (2008).